Bound states of defects in superconducting LiFeAs studied by scanning tunneling spectroscopy

S. Grothe,[1,2] Shun Chi,[1,2] P. Dosanjh,[1,2] Ruixing Liang,[1,2] W. N. Hardy,[1,2] S. A. Burke,[1,3,2] D. A. Bonn,[1,2] and Y. Pennec[1,2]

[1]*Department of Physics and Astronomy, University of British Columbia, Vancouver, British Columbia, Canada V6T 1Z1*

[2]*Quantum Matter Institute, University of British Columbia, Vancouver, British Columbia, Canada V6T 1Z4*

[3]*Department of Chemistry, University of British Columbia, Vancouver, British Columbia, Canada V6T 1Z1*

(Received 18 July 2012; revised manuscript received 14 September 2012; published 5 November 2012)

Defects in LiFeAs are studied by scanning tunneling microscopy and spectroscopy (STS). Topographic images of the five predominant defects allow the identification of their positions within the lattice. The most commonly observed defect is associated with an Fe site and does not break the local lattice symmetry, exhibiting a bound state near the edge of the smaller gap in this multigap superconductor. Three other common defects, including one also on an Fe site, are observed to break local lattice symmetry and are pair breaking, indicated by clear in-gap bound states, in addition to states near the smaller gap edge. STS maps reveal complex, extended real-space bound-state patterns, including one with a chiral distribution of the local density of states. The multiple bound-state resonances observed within the gaps and at the inner gap edge are consistent with theoretical predictions for the $s^{\pm}$ gap symmetry proposed for LiFeAs and other iron pnictides.

DOI: 10.1103/PhysRevB.86.174503 PACS number(s): 74.55.+v, 74.70.Xa, 74.62.Dh, 72.10.Fk

I. INTRODUCTION

Impurity physics plays a key role in superconducting systems, beginning with the remarkable feature that nonmagnetic defects do not strongly impact superconductivity in conventional s-wave materials.[1] In contrast to such single-sign s-wave superconductors, where only magnetic defects cause pair breaking and in-gap states,[2] both potential and magnetic defects can induce in-gap states in d-wave[3–5] and multiband sign-reversal s-wave superconductors ($s^{\pm}$).[6–9] Not surprisingly then, a superconductor's sensitivity to defects plus the energetic and spatial characterization of bound states localized at defect sites have provided clues to the pairing symmetry of superconductors, and scanning tunneling microscopy (STM) and spectroscopy (STS) have proven invaluable tools for such studies.[4,5,10,11] Since a sign change of the order parameter gives rise to sensitivity to defects, it has been suggested that the study of these impurity bound states in the iron arsenides could help close the ongoing discussion regarding the gap structure (s^{++} or $s^{\pm}$).[7–9]

The fact that most high-temperature superconductors, cuprates as well as pnictides, require chemical substitutions to tune them into their superconducting states adds further importance to understanding the effect of defects in these systems.[12] In the cuprates, this tuning is often achieved through cation substitution on sites away from the CuO_2 planes, doping them with holes or electrons, while largely avoiding strong scattering. Direct substitution onto the CuO_2 planes is typically pair breaking, sometimes strongly, sometimes weakly.[13] For many iron-based superconductors chemical substitution that suppresses extended magnetic order is an essential ingredient in achieving high-temperature superconductivity.[14] In $BaFe_2As_2$ it has been shown that certain elements such as Co and Ni substituted into the Fe layer induce superconductivity[15,16] while other substituents (Mn) cause strong pair breaking.[17] Thus, the arsenides lack the easy distinction of off-plane substitution to promote superconductivity versus on-plane defects that are pair breaking. This makes it particularly important to assess individual impurities and their influence on the surrounding electronic states.

STM study of the pnictides has proven difficult due to surface-specific effects arising from a lack of natural cleaving planes, or from structural or electronic reconstruction caused by a polar catastrophe.[18] Recently, stoichiometric examples within the pnictide and chalcogenide families that exhibit surfaces suitable for STM study, such as cleaved LiFeAs crystals[19] and films of FeSe (Ref. 20) and KFe_2Se_2 (Ref. 21) grown by molecular beam epitaxy, have presented the opportunity to apply STM and STS to well-defined systems. All three also possess the advantage of being superconducting without chemical substitutions. In LiFeAs, STM has been used to measure the superconducting gaps of clean defect-free areas,[22,23] to study vortices,[23] and to determine band structure and gap symmetry through quasiparticle interference induced by defect scattering.[24,25] A detailed investigation of the impurities themselves and their localized electronic effects has yet to be reported, though in-gap states have been observed for iron adatoms in FeSe,[26] and possibly iron vacancies in KFe_2Se_2.[21]

In this paper we characterize defects arising from crystal growth in nominally stoichiometric LiFeAs. We identify their positions in the crystal lattice and analyze the spatial and energetic distribution of their bound states.

II. EXPERIMENTAL METHOD

The LiFeAs single crystals were grown by the LiAs self-flux technique. Li_3As was presynthesized through the reaction of Li (99.9%) lumps and As (99.9999%) powder at 773 K for 10 h. FeAs was presynthesized from mixed powders of Fe (99.995%) and As (99.9999%) at 973 K for 10 h. Powders of Li_3As and FeAs were mixed in a composition of 1:2 and placed in an alumina crucible, which was sealed under 0.3 atm Ar in a quartz tube. A Mo crucible was used to encapsulate the alumina crucible to prevent Li attack on the quartz tube. All the mixing procedures were done in an Ar-atmosphere glovebox. The mixture was heated slowly to 1323 K for 10 h, and then cooled to 1073 K at 4.5 K/h. Finally, the samples were additionally annealed at 673 K for 12 h before being removed

from the furnace. Single crystals with typical dimensions $2 \times 2 \times 0.2$ mm^3 were mechanically extracted from the LiAs flux. The lattice parameters $a = (3.777 \pm 0.004)$ Å and $c = (6.358 \pm 0.001)$ Å were determined by x-ray diffraction, and $T_c^{\text{onset}} = 17$ K with a transition width of 1 K was determined by superconducting quantum interference device (SQUID) magnetometry with a 1 G magnetic field.

STM and STS measurements were performed in a Createc ultrahigh-vacuum low-temperature STM. The electrochemically etched tungsten tip was Ar sputtered and thermally annealed at the beginning of this experiment. After cleaving the sample *in situ* at a temperature of 20 K it was immediately transferred to the 4.2 K STM. The sample is identical to the one used in a previous study,[22] but it was recleaved before we obtained the measurements presented here. All spectra shown in this report were recorded at a temperature of 2.2 K and were acquired by numerical differentiation of the I-V sweep. All topography scans and dI/dV maps were recorded at 4.2 K.

III. RESULTS AND DISCUSSION

Figures 1(a) and 1(c) to 1(e) show atomic-resolution topographic images with common types of defects at the surface of LiFeAs. Defects with similar topography and densities have been observed in STM studies of LiFeAs grown elsewhere.[23,24] STM scans of LiFeAs also show other types of defects, but we decided to focus on the most common ones with the largest effect on the electronic structure. For a clear identification of the Fe, Li, and As positions, and thereby assignment of the visible defect sites, a close look at the crystallography and the defects is needed.

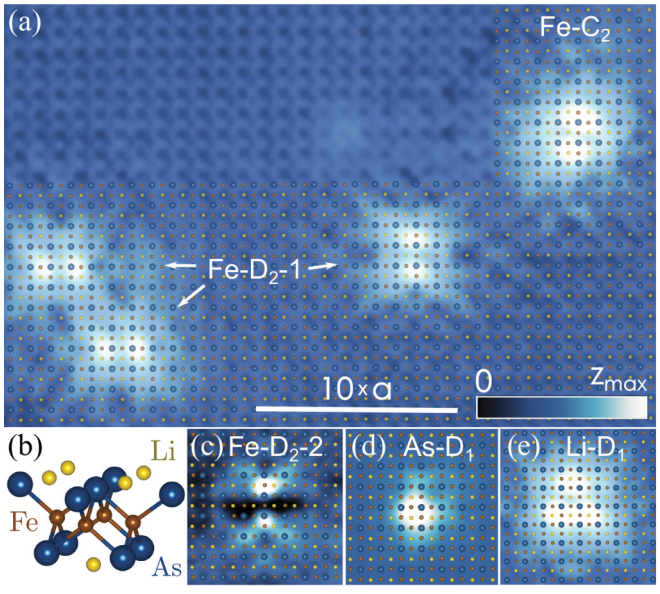

FIG. 1. (Color) Scanning tunneling topographies of typical defects found at the surface of LiFeAs. The estimated atomic configuration of the crystal structure with $a = (3.74 \pm 0.03)$ Å(Ref. 22) is shown on top of the topographies to locate the defect positions (Li, yellow; As, blue; Fe, red). (a) Three different Fe-D_2-1 and one Fe-C_2 defect. (b) Schematic crystal structure in edge-on view of the upper layers of LiFeAs with Li at the top as expected from cleaving. (c),(d),(e) Topographies of Fe-D_2-2, As-D_1, and Li-D_1 defects. The tunneling conditions were $I_T = 100$ pA for all scans and $U_B = 6$ meV, $z_{\max} = 120$ pm [(a) and (e)], $U_B = -12$ meV, $z_{\max} = 55$ pm (c), and $U_B = -12$ meV, $z_{\max} = 120$ pm (d).

LiFeAs presents a layered crystal structure detailed in Fig. 1(b).[19] At its core is a square lattice of Fe atoms, each nested at the center of a tetrahedron of As. After cleaving between the weakly bonded Li layers, the surface consists of a top layer of Li in a square lattice followed by a square lattice of As of the same periodicity but translated by [1/2,1/2]. The third layer is Fe arranged again in a square lattice but of twice the density and rotated 45° relative to the Li or As lattice, where neither As nor Li sits directly above or below an Fe site.

The most common defect [labeled Fe-D_2-1 in Fig. 1(a) according to labeling principles described below] provides a key clue to the identification of the lattice observed by STM. Its distinctive feature is the dihedral D_2 symmetry, exhibiting two bright lobes oriented along either [100] or [010]. The symmetries discussed in this work are based on the Schönfließ notation adapted for two dimensions, since STM provides a weighted two-dimensional (2D) projection of the 3D crystal most sensitive to disruptions occurring on the upper rather than the buried planes.

The question is which chemical site in the lattice can generate the observed topography? To form the center of this D_2 defect, both the Li and As sites are unlikely as they present D_4 symmetry due to the four nearest neighbors within each plane as discussed above. Iron sites, however, would induce a D_2 symmetry in the upper planes due to the tetrahedrally bonded As nearest neighbors with two As atoms in the plane above and two in the plane below [Fig. 1(b)]. Therefore, the simplest explanation for this commonly observed defect is an iron-site defect, even though other origins such as dimers or interstitial impurities cannot be completely excluded. The four strongly polarizable nearest-neighbor As atoms[27] would be most significantly affected by an iron-site defect through charge transfer. But STM is much more sensitive to changes on the upper two As atoms above the Fe layer, resulting in a prominent charge density contrast along the direction of these two As atoms. Likely this defect arises from Fe vacancies or Li substitution at iron sites, as the crystal was grown from a Li-rich flux. In the following we refer to this defect as Fe-D_2-1 based on the apparent center position and symmetry.

The spatial assignment of the Fe-D_2-1 defect, centered on an iron site and extended along the line of the two As nearest neighbors lying above the Fe layer, allows the registry of the three atomic sublattices (Fe, As, and Li) to the measured STM corrugation. In Fig. 1(a) the STM topography is overlaid with a model of the (001) cleaved crystal structure of LiFeAs (Li, yellow; As, blue; and Fe, orange), where the Fe site is at the center of the Fe-D_2-1 defect and the two topmost As atoms are located at the lobes. This model works remarkably well across the full scan with no phase shift between the applied grid and the measured atomic periodicity matching the Fe periodicity.

Previously, atomic-resolution STM images of LiFeAs have produced the periodicity of either Li or As.[22–25] Here, the periodicity of the Fe lattice is observed at low bias voltages ($|U_B| \lesssim 20$ meV) and with a particular tip wave function, which also causes a stronger weight of the small superconducting gap in STS. A typical STS spectrum taken at the center of a defect-free area is shown in Fig. 2(a) in

solid black. As reported previously,[22–24] two nodeless gaps are clearly resolved with half-width peak to peak of $\Delta_1^{pp} = 6$ meV and half-width shoulder to shoulder $\Delta_2^{pp} = 3$ meV, but the spectral weight contribution of the small gap Δ_2 is about twice as large as previously found.[22] The STM quasiparticle interference study by Allan *et al.* identified the small energy gap with a size of about 2 to 3 meV and a negative dispersion as being associated with the outer hole pocket,[24] which also corresponds to the in-plane Fe-d_{xy} orbital.[28–30] Tunneling into the electron pockets which have d_{xy}, d_{xz}, and d_{yz} character and which contain the other two gaps[28–30] cannot be completely excluded but is expected to be strongly suppressed because of the larger in-plane momentum $|\vec{k}_{||}|$.[31] Thus we conclude that the sensitivity to the iron corrugation observed here is combined with an enhanced tunneling into the iron in-plane d_{xy} orbital.[32]

Turning to the effect of the Fe-D_2-1 defect on the local density of states (LDOS) in the vicinity of the defect, the energetic and spatial distributions of bound states are revealed. Figure 2(a) (upper panel) shows two raw spectra taken at 2.2 K at the center and on the lobes of the Fe-D_2-1 defect as well as a reference spectrum of pristine LiFeAs, taken from the same region. The lower panel presents these two spectra normalized by subtracting the reference to enhance subtle features.[33] The first effect of the defect is a suppression of spectral weight at the large-gap coherence peaks. More interestingly, both spectra reveal a resonance at 3 meV coinciding with the edge of the small gap Δ_2^{pp} and slightly more pronounced at the lobe than at the defect center. Δ_2 is on a Fermi surface segment dominated by the iron in-plane d_{xy} band, expected to be influenced by defects in the iron plane. A bias-symmetric counterpart at -3 meV is not visible within our resolution. The 4.2 K spatial distribution of the 3 meV bound-state resonance, shown in Fig. 2(c), follows the D_2 pattern measured in topography. To enhance spatial features, the maps were averaged over the 2 meV width of the bound state, i.e., from 2 to 4 meV for the 3 meV map.

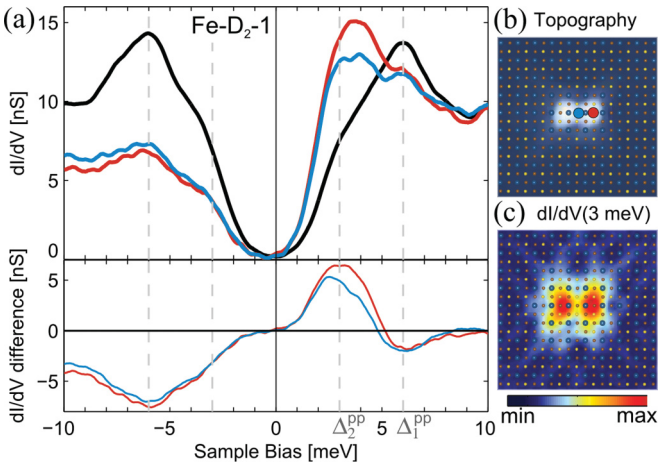

FIG. 2. (Color) (a) Upper panel: dI/dV spectra taken at a Fe-D_2-1 defect (red and blue lines) and the average over 20 spectra measured about 2 nm away from the defect (black line). Lower panel: The thin red and blue lines correspond to the difference between the spectra taken at the defect and the average from the defect-free position. A bound state is visible at approximately 3 meV. Spectra were taken at the positions marked by single red and blue dots in the topographic image (b). (c) dI/dV map at an energy of 3 ± 1 meV, i.e., averaged from 2 to 4 meV. The topography and the dI/dV maps are overlaid with the top-view crystal structure. Spectra shown in (a) were taken at a temperature of 2.2 K. Topography and dI/dV map shown in (b) and (c) were recorded at 4.2 K with a constant tip-sample separation defined by $U_{B,0} = 25$ meV, $I_0 = 260$ pA. Topography and dI/dV maps have edge lengths of ≈3.4 nm.

We now address four other recurrent defects of LiFeAs which we register based on our identification of the lattice as shown in Figs. 1(a) and 1(c)–1(e). A second Fe-centered defect also has a dihedral D_2 symmetry and is referred to as Fe-D_2-2 [Fig. 1(c)]. Fe-D_2-2, which we will not discuss in detail, exhibits similar electronic properties to Fe-D_2-1 but with a weaker 3 meV bound-state resonance. The others are labeled Fe-C_2, Li-D_1, and As-D_1 based on the apparent defect-site registry in the xy plane and their two-dimensional group symmetry. We note that the center position of the Li-D_1 and As-D_1 defects is somewhat ambiguous due to their large and complex spatial extents. Here the notation gives the regular lattice position closest to the apparent defect center. We observed the two possible chiralities and two orientations of Fe-C_2 as well as all four possible orientations of Li-D_1 and As-D_1. We note that except for the two Fe-D_2 defects, the other three break the local symmetry of the crystal lattice. This symmetry breaking can be caused by particular orbital orientations close to the defect,[34] by interstitial impurity positions or by the occurrence of two or more impurities close to each other. A summary of the defect characteristics is presented in Table I.

Figure 3(a) shows spectra taken at the center and the arm of an As-D_1 defect. Like Fe-D_2-1, As-D_1 causes a strong suppression of the coherence peaks of Δ_1. However, the spectra not only reveal a resonance close to the positive edge of Δ_2 but also indicate a peak below $-\Delta_2$ at about -3.7 meV. Additionally, another resonance appears inside the gap at about -1.5 meV. The -1.5 meV resonance is present only in the arm of the defect but not at its center. This is made clearer by the

TABLE I. Summary of the five defect types. The approximate density is the number per LiFeAs formula unit and has been obtained for one sample cleaved twice. Other samples have shown the same types of defects, with similar relative densities, but sample-to-sample differences of absolute densities. E_b is the bound-state energy relative to E_F. The asterisk indicates those defects where the spatial assignment is ambiguous.

Defect	Symmetry	Density (10^{-3})	E_b (meV)	$\frac{\lvert E_b\rvert}{\Delta_1^{pp}}$	$\frac{\lvert E_b\rvert}{\Delta_2^{pp}}$
Fe-D_2-1	D_2	$\gtrsim$1.2	≈3.0	0.5	1
Fe-D_2-2	D_2	$\lesssim$0.2	≈3.0	0.5	1
As-D_1(*)	D_1	$\lesssim$0.5	≈3.7	0.62	1.23
			≈−1.5	0.25	0.5
Li-D_1(*)	D_1	$\lesssim$0.1	≈3.7	0.62	1.23
			≈1.2	0.2	0.4
Fe-C_2	C_2	$\lesssim$0.1	≈±3.5	0.58	1.17
			≈1.0	0.17	0.33

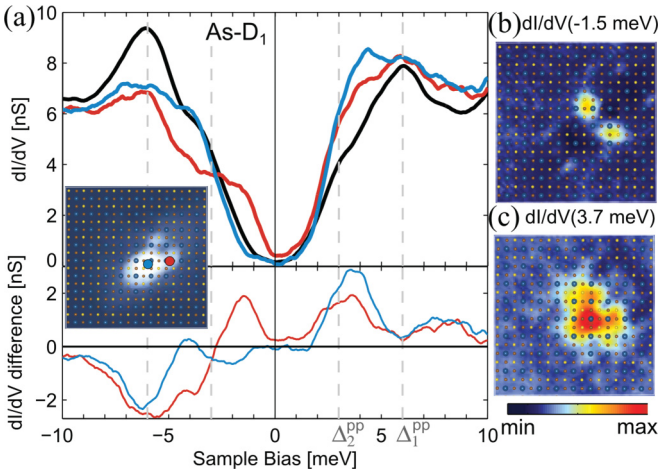

FIG. 3. (Color) As Fig. 2 but for the As-D_1 defect. Bound states are visible at approximately -1.5 meV and at $+3.7$ meV. The topography which indicates the location of the spectra is shown as an inset of (a). (b),(c) dI/dV maps at energies of -1.5 and 3.7 ± 1 meV, respectively.

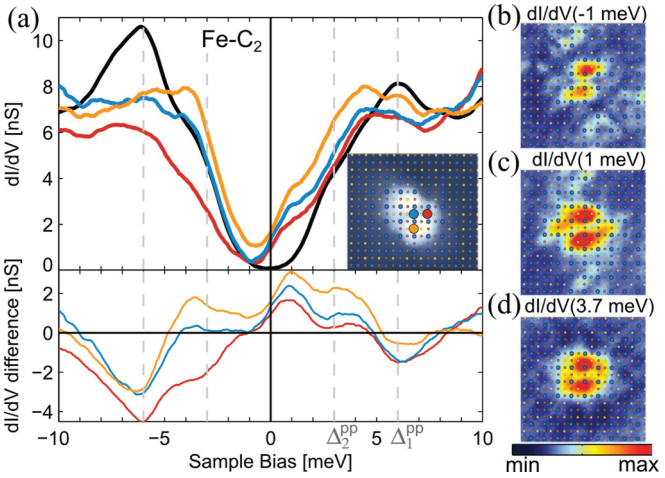

FIG. 5. (Color) As Fig. 2 but for the Fe-C_2 defect. (a) Bound states are visible at approximately +1.0 meV and at about ± 3.5 meV. The topography which indicates the location of the spectra is shown as an inset of (a). (b),(c),(d) dI/dV maps at energies of -1, 1, and 3.7 ± 1 meV, respectively.

spectral maps acquired at -1.5 meV and 3.7 meV presented in Figs. 3(b) and 3(c).

Spectra taken on the Li-D_1 defect are shown in Fig. 4(a). Again, the coherence peaks of the large gap are reduced but a resonance near Δ_2 is just weakly suggested. The three spectra in Fig. 4(a) are qualitatively similar, showing a clear in-gap resonance at about 1.2 meV. Spectral maps at 1 meV, at the bias-symmetric energy -1 meV, and at the 3.7 meV peak just above Δ_2 are shown in Figs. 4(b), 4(c), and 4(d), revealing that the near 1 meV state is the most extended. At -1 meV, the LDOS is predominantly localized on two As sites near the Li center.

Figure 5(a) shows spectra recorded on three sites of an Fe-C_2 defect. Once more, the defect reduces the amplitude of the coherence peaks of Δ_1. Resonances at 1 meV and approximately ± 3.5 meV are observed. The spatial dI/dV mapping of these defects differs from the constant-current

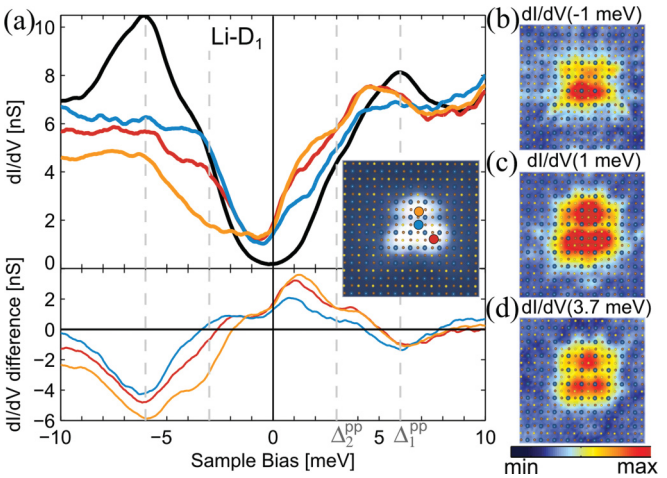

FIG. 4. (Color) As Fig. 2 but for the Li-D_1 defect. (a) A bound state is visible at approximately +1.2 meV. The topography which indicates the location of the spectra is shown as an inset of (a). (b),(c),(d) dI/dV maps at energies of -1, 1, and 3.7 ± 1 meV, respectively.

map topography. The dI/dV map at the -3.5 meV resonance (not shown) is qualitatively similar to the -1 meV map. Interestingly, the -1 meV and 3.7 meV maps show one chirality while the opposite chirality is observed at $+1$ meV [Figs. 5(b)–5(d)].

Summarizing the properties of all defects, some striking features of the dI/dV maps presented here should be highlighted. Bound-state resonances exhibit large spatial extents, most distinct within an area of $\sim 4 \times 4$ unit cells. Three of the five defect types observed in LiFeAs break the lattice symmetry and the bound-state patterns are not commensurate with the crystal lattice. The strong dependence on the bias voltage reveals different spatial localization of different resonance energies. Consequently, bound states in LiFeAs result in more complex patterns than those observed in the cuprates where the LDOS of particle and hole components shows complementary patterns overlaying the CuO lattice sites.[5] In particular, the chiral C_2 pattern of the Fe-C_2 defect is rarely observed. A recent similar observation in $NbSe_2$ is attributed to charge density waves,[35] and it has been recently proposed that impurities in pnictides may yield chiral C_2 LDOS patterns in the presence of spin density order[36] or strong orbital fluctuations.[37] If the extraordinary chiral pattern of the Fe-C_2 defect is indeed connected to magnetic, charge, or orbital order locally frozen by the defect, the present observations might provide further insight regarding the pairing glue in LiFeAs.

We turn to the analysis of bound-state energies relative to the gap sizes, which can help to identify the gap structure. Both of the two lattice-symmetry-preserving Fe-D_2 defects stand out as having only one bound state appearing near the edge of the small gap. As-D_2, Li-D_1, and Fe-C_2 also cause resonances at or near the small gap edge Δ_2, but lower-temperature measurements are needed to clearly resolve these features. As-D_2, Li-D_1, and Fe-C_2, which break the local lattice symmetry, induce pair breaking indicated by clear in-gap bound states pronounced at either positive or negative bias. For most resonances only one peak is visible and the expected bias-symmetric counterpart[7–9] is either not

observed or only weakly present, revealing a significant particle-hole asymmetry of the bound states as observed by STS. Due to our resolution and the uncertainty inherent in finding the bound-state peaks on a background that is also influenced by the presence of the defect, we cannot definitively ascribe these states to the small gap edge, and cannot exclude that they are in-gap states of the larger gap. However, the asymmetric multipeak energetic structure we observe and the observation of states near the small gap are consistent with recent theoretical predictions for $s^{\pm}$ symmetries.[7,9] While we cannot exclude the possibility that the defects in the crystal exhibit magnetic properties, potentially inducing in-gap bound states for either $s^{\pm}$ or s^{++},[7,8] such states at the gap edge have not previously been observed in conventional s-wave superconductors.[10,11,38] Controlled introduction of impurities and probing of the bound-state resonances should provide further evidence for the pairing symmetry in the iron pnictides.

Regardless of pairing symmetry and interaction, we gain information regarding the resilience of the superconductive phase of LiFeAs to chemical substitution within the iron layer, reminiscent of the observation of pair-breaking and non-pair-breaking Fe-site defects in $BaFe_2As_2$.[15–17] Even though all common LiFeAs defects show bound states within the large gap Δ_1, the two Fe-D_2 defects have no states within Δ_2, raising the question of how defects affect charge carriers in different bands. In contrast, Fe-C_2, with its bound state below both gaps, clearly corresponds to a pair-breaking substituent also likely located within the iron layer.

IV. CONCLUSION

We classify and register the common defects appearing at the surface of LiFeAs. Our registry can be used as a guideline for the identification of deliberately introduced external impurities. The bound states show complex spatial patterns that vary strongly with energy and do not reflect the lattice periodicity. Further, the energetic multipeak bound-state structures with resonances at the small superconducting gap are in accordance with calculations of nonmagnetic defects in $s^{\pm}$ gap structures,[9] although the possibility of a magnetic nature of our defects does not allow a definitive attribution of the gap structure. Finally, the observed variety of different defects suggests many possibilities for controlled doping and thereby for tailoring the material properties.

ACKNOWLEDGMENTS

The authors would like to thank Ilya Elfimov, George Sawatzky, and Giorgio Levy for several helpful conversations. This work was supported by the Canadian Institute for Advanced Research, the Canada Foundation for Innovation, and the Natural Sciences and Engineering Research Council of Canada.

[1] P. W. Anderson, J. Phys. Chem. Solids **11**, 26 (1959).
[2] L. Yu, Acta Phys. Sin. **21**, 75 (1965); H. Shiba, Prog. Theor. Phys **40**, 435 (1968).
[3] A. V. Balatsky, M. I. Salkola, and A. Rosengren, Phys. Rev. B **51**, 15547 (1995).
[4] A. Yazdani, C. M. Howald, C. P. Lutz, A. Kapitulnik, and D. M. Eigler, Phys. Rev. Lett. **83**, 176 (1999).
[5] S. H. Pan, E. W. Hudson, K. M. Lang, H. Eisaki, S. Uchida, and J. C. Davis, Nature (London) **403**, 746 (2000); E. W. Hudson, K. M. Lang, V. Madhavan, S. H. Pan, H. Eisaki, S. Uchida, and J. C. Davis, *ibid.* **411**, 920 (2001).
[6] G. Preosti and P. Muzikar, Phys. Rev. B **54**, 3489 (1996).
[7] D. Zhang, Phys. Rev. Lett. **103**, 186402 (2009).
[8] W.-F. Tsai, Y.-Y. Zhang, C. Fang, and J. Hu, Phys. Rev. B **80**, 064513 (2009).
[9] T. Kariyado and M. Ogata, J. Phys. Soc. Jpn. **79**, 083704 (2010).
[10] A. Yazdani, B. A. Jones, C. P. Lutz, M. F. Crommie, and D. M. Eigler, Science **275**, 1767 (1997).
[11] S.-H. Ji, T. Zhang, Y.-S. Fu, X. Chen, X.-C. Ma, J. Li, W.-H. Duan, J.-F. Jia, and Q.-K. Xue, Phys. Rev. Lett. **100**, 226801 (2008).
[12] J. G. Bednorz and K. A. Müller, Z. Phys. B **64**, 189 (1986); Y. Kamihara, T. Watanabe, M. Hirano, and H. Hosono, J. Am. Chem. Soc. **130**, 3296 (2008).
[13] H. Alloul, J. Bobroff, M. Gabay, and P. J. Hirschfeld, Rev. Mod. Phys. **81**, 45 (2009).
[14] H. Wadati, I. Elfimov, and G. A. Sawatzky, Phys. Rev. Lett. **105**, 157004 (2010).
[15] A. S. Sefat, R. Jin, M. A. McGuire, B. C. Sales, D. J. Singh, and D. Mandrus, Phys. Rev. Lett. **101**, 117004 (2008).
[16] L. J. Li, Y. K. Luo, Q. B. Wang, H. Chen, Z. Ren, Q. Tao, Y. K. Li, X. Lin, M. He, Z. W. Zhu, G. H. Cao, and Z. A. Xu, New J. Phys. **11**, 025008 (2009).
[17] A. Thaler, H. Hodovanets, M. S. Torikachvili, S. Ran, A. Kracher, W. Straszheim, J. Q. Yan, E. Mun, and P. C. Canfield, Phys. Rev. B **84**, 144528 (2011).
[18] J. E. Hoffman, Rep. Prog. Phys. **74**, 124513 (2011).
[19] J. H. Tapp, Z. Tang, B. Lv, K. Sasmal, B. Lorenz, P. C. W. Chu, and A. M. Guloy, Phys. Rev. B **78**, 060505 (2008); X. C. Wang, Q. Q. Liu, Y. X. Lv, W. B. Gao, L. X. Yang, R. C. Yu, F. Y. Li, and C. Q. Jin, Solid State Commun. **148**, 538 (2008); M. J. Pitcher, D. R. Parker, P. Adamson, S. J. C. Herkelrath, A. T. Boothroyd, R. M. Ibberson, M. Brunelli, and S. J. Clarke, Chem. Commun. **2008**, 5918 (2008).
[20] F. C. Hsu, J.-Y. Luo, K.-W. Yeh, T.-K. Chen, T.-W. Huang, P. M. Wu, Y.-C. Lee, Y.-L. Huang, Y.-Y. Chu, D.-C. Yan, and M.-K. Wu, Proc. Natl. Acad. Sci. USA **105**, 14262 (2008).
[21] W. Li, H. Ding, P. Deng, K. Chang, C. Song, K. He, L. Wang, X. Ma, J.-P. Hu, X. Chen, and Q.-K. Xue, Nat. Phys. **8**, 126 (2011).
[22] S. Chi, S. Grothe, R. Liang, P. Dosanjh, W. N. Hardy, S. A. Burke, D. A. Bonn, and Y. Pennec, Phys. Rev. Lett. **109**, 087002 (2012).
[23] T. Hanaguri, K. Kitagawa, K. Matsubayashi, Y. Mazaki, Y. Uwatoko, and H. Takagi, Phys. Rev. B **85**, 214505 (2012).
[24] M. P. Allan, A. W. Rost, A. P. Mackenzie, Yang Xie, J. C. Davis, K. Kihou, C. H. Lee, A. Iyo, H. Eisaki, and T.-M. Chuang, Science **336**, 563 (2012).
[25] T. Hänke, S. Sykora, R. Schlegel, D. Baumann, L. Harnagea, S. Wurmehl, M. Daghofer, B. Büchner, J. van den Brink, and C. Hess, Phys. Rev. Lett. **108**, 127001 (2012).

[26]C. L. Song, Y.-L. Wang, P. Cheng, Y.-P. Jiang, W. Li, T. Zhang, Z. Li, K. He, L. Wang, J.-F. Jia, H.-H. Hung, C. Wu, X. Ma, X. Chen, and Q.-K. Xu, Science **332**, 1410 (2011).

[27]M. Berciu, I. Elfimov, and G. A. Sawatzky, Phys. Rev. B **79**, 214507 (2009).

[28]S. V. Borisenko, V. B. Zabolotnyy, A. A. Kordyuk, D. V. Evtushinsky, T. K. Kim, I. V. Morozov, R. Follath, and B. Büchner, Symmetry **4**, 251 (2012).

[29]J. Ferber, K. Foyevtsova, R. Valentí, and H. O. Jeschke, Phys. Rev. B **85**, 094505 (2012).

[30]T. Hajiri, T. Ito, R. Niwa, M. Matsunami, B. H. Min, Y. S. Kwon, and S. Kimura, Phys. Rev. B **85**, 094509 (2012).

[31]J. Tersoff and D. R. Hamann, Phys. Rev. Lett. **50**, 1998 (1983).

[32]The energetic positions of bound-state resonances are not expected to be influenced by the tip state, which we have confirmed by comparing the data shown here for the Fe-D_2-1 with 4 K spectra on this defect from our previous data (Ref. 22), showing the lower weight of Δ_2.

[33]We note that this normalization procedure may slightly shift energetic features especially if there is an overall redistribution of spectral weight, a gap suppression, or multiple peaks that are within our 200 μV resolution. Since these factors likely exceed the small statistical uncertainty of locating the peak position, we report only approximate values for bound-state energies.

[34]H. Amara, S. Latil, V. Meunier, Ph. Lambin, and J.-C. Charlier, Phys. Rev. B **76**, 115423 (2007).

[35]J. Ishioka, T. Fujii, K. Katono, K. Ichimura, T. Kurosawa, M. Oda, and S. Tanda, Phys. Rev. B **84**, 245125 (2011).

[36]H. Huang, Y. Gao, D. Zhang, and C. S. Ting, Phys. Rev. B **84**, 134507 (2011).

[37]Y. Inoue, Y. Yamakawa, and H. Kontani, Phys. Rev. B **85**, 224506 (2012).

[38]A. V. Balatsky, I. Vekhter, and J.-X. Zhu, Rev. Mod. Phys. **78**, 373 (2006).